Surprising Decrease in the Martian He Bulge during PEDE-2018 and Changes in Upper Atmospheric Circulation

Meredith K. Elrod[1,2], Stephen Bougher[3], Kali Roeten[3], Kenneth Arnold[1]

[1] CRESST II, University of Maryland College Park, College Park, MD, USA
[2] Planetary Environments Lab, Code 690, NASA Goddard Space Flight Center, Greenbelt, MD, USA
[3] Department of Climate and Space Sciences and Engineering, University of Michigan, Ann Arbor, MI, USA

Key Points: (140 characters)

- He collects in the upper atmosphere above the dawn winter polar atmosphere region.

- He bulge density is unexpectedly lower in MY 34 northern winter during the (PEDE) than other observed northern winter during MY 32 & 35.

- He is a tracer for upper atmosphere circulation and changes in the bulge indicate the circulation changed as shown through modeling.

Abstract (250 words)

Using the Neutral Gas and Ion Mass Spectrometer (NGIMS) on the Mars Atmosphere Volatile and Evolution spacecraft (MAVEN) we analyzed data from Mars Year (MY) 32, 34, and 35 to examine the He bulge during the northern winter solstice (Ls ~180-240) specifically focusing on the effects from the planet encircling dust event (PEDE-2018). He collects on the dawn/nightside winter polar hemisphere of Mars. The seasonal migration of the He bulge has been observed and modeled (Elrod, et al., 2017; Gupta, et al., 2021). The MAVEN orbit precesses around Mars allowing for a variety of latitude and local time observations throughout the Martian year. MY 32, 34, and 35 had the best possible opportunities to observe the He bulge during northern winter (Ls ~180-240). NGIMS observations during MY 32 and MY 35 revealed a He bulge on the nightside to dawn in alignment with modeling and previous publications. However, in MY 34, during the PEDE, the He bulge was not present indicating the PEDE directly impacted upper atmospheric circulation. Updates in modeling indicate changes in circulation and winds can cause He to shift further north than MAVEN was able to observe. While adding a simple static version of gravity waves to the Mars Global Ionosphere Thermosphere Model (M-GITM) model may account for some of the variations in the global circulation during the dust event, other studies (e.g., Yiğit, E, 2023) have posited that the gravity waves during the dust storm were more variable that the initial parameters we have included.

Plain Language Summary (200 words)

Mars is regularly subject to large dust storms that typically start during the northern winter season. Approximately every 7-10 years these large storms can merge and grow and become planet sized dust storms that cover 80-95% of the surface. These rare and massive planet sized storms last for about a month before slowly dissipating, changing not only the surface of the planet but also the structure and composition of the atmosphere. Mars has regular helium bulges that collect in the cold part of the upper atmosphere (e.g., polar winter regions on the night, dawn side). Global circulation models of the atmosphere have shown this helium bulge as predictable throughout the Martian year. The Mars Atmospheres and Volatiles EvolutioN (MAVEN) spacecraft made observations of Helium over the course of 4 Martian years, but during the last major global dust storm, where a Helium bulge in the upper atmosphere should have been observed, no increase in Helium associated with a bulge was observed. This could have implications for the broader impact of regular global dust storms, winds, and upper atmosphere circulation on the Martian atmosphere.

1. Introduction

In late May/early June of 2018 the Mars Reconnaissance Orbiter (MRO) Mars Climate Sounder (MCS) detected the onset of a large dust storm system near the equator. This storm system grew and merged with other dust storms forming at the same time and by 3 June (Ls ~186) 2018, MRO/MCS declared the storm system to be a planet encircling dust event (PEDE). By 8 June (Ls ~189) the PEDE was detectable in the upper atmosphere by multiple orbiting spacecraft including MRO (Wolkenberg, et al., 2020; Kass, et al., 2020; Elrod, et al., 2020; Jain, et al., 2020; Rao, et al., 2020; Felici, et al., 2020). The PEDE peaked by 7-13 July (Ls ~207-210) as

determined by zonally averaged temperatures observed by MRO/MCS in the middle atmosphere (Kass, et al., 2020). The PEDE maximum correlates with the highest optical depth and largest increase in densities and scale heights in the upper atmosphere as measured by Mars Atmosphere and Volatiles EvolutioN (MAVEN) Neutral Gas and Ion Mass Spectrometer (NGIMS) (Elrod, et al., 2020). The dust storm lasted for a little over a month with the decay occurring around mid-September allowing the atmosphere to show signs of returning to seasonal and diurnal normal (Ls ~180 - 240).

Helium, a light element, has a large scale height (H) in the upper atmosphere like hydrogen, but it has the uniqueness of being non-reactive, so it is not influenced by chemistry with carbon and oxygen in the atmosphere. This allows He to become a tracer for the atmospheric circulation. Being much lighter than the bulk of the atmosphere, He will pool in the colder, condensed, parts of the atmosphere, typically the winter polar dawn region near solstices and equinoxes at mid-to- high latitudes. This light species transport occurs by the process of wind-induced diffusion (e.g., Mayr, et al., 1978; 1980) that occurs on Earth and Venus as well. Previous studies of the He in the upper atmosphere of Mars have shown an agreement with this behavior (Elrod, et al., 2017; Gupta, et al., 2021). Mars Year 34 was an exception. While MAVEN was in a good position to be able to observe the winter polar dawn side He bulge, there was no He bulge observed. This sampling period was different because MY 34 encountered a Planet Encircling Dust Event (PEDE). Studies are emerging that the dynamics, heating, composition, and chemistry in the upper atmosphere were all modified during the global dust storm (e.g., Elrod, et al., 2020; Stone S. W., et al., 2020; Jain, et al., 2020).

The impact of the global dust storm has been shown to have an increase in water ice at higher altitudes than previously measured (Stone S. W., et al., 2020) along with compositional changes to the upper atmosphere (Elrod, et al., 2020; Farahat, et al., 2021). The compositional changes in the upper atmosphere indicated that the lighter species, specifically the O and N_2 were reduced during the PEDE compared to the main species (CO_2 and Ar). Examination of the nightside winter and dusk data taken by MAVEN/NGIMS during the PEDE revealed that the He density was lower than what had been previously observed for the He bulge during winter solstice observations. (see Elrod, et al., 2017; Gupta, et al., 2021; and, figure1).

Mars has a He bulge (Elrod, et al., 2017) that peaks in density where the temperatures of the upper atmosphere are relatively cool. MAVEN/NGIMS has obtained in-situ observations of He for 5 Mars Years (MY), MY 32 – 36. He density peaks are highest around equinox (Ls ~0, or 180) near mid to high latitudes (lat ~45-70º) and winter solstice (Ls ~90 or 270) near corresponding high latitudes (lat ~55-80) on the night or dawn side local solar time (LST) of ~22-5 h. Due to the eccentricity of the Martian orbit, there is some observed asymmetry between the northern and southern He bulge (Gupta,et al., 2021).

In order for NGIMS to be able to observe the He bulge, because it is an in-situ instrument, MAVEN needs to be moving through the He bulge. Therefore, in order to follow the northern winter He bulge, we need to constrain our observations to those when MAVEN is in the northern hemisphere from Ls 180-280. Since the He bulge is constrained from LST 22-6h (midnight to dawn) if NGIMS is only observing on the dayside during this period, then a Helium bulge is not likely to be observed. MAVEN was in the northern hemisphere from Ls 180-280 in MY 32, 34, and 35. In all three years, NGIMS observed from midnight to dawn within this Ls

range. In MY 33 and 36 MAVEN was in the southern hemisphere from Ls 180-280, making it impossible for NGIMS to detect the winter He bulge at this time. For this reason, we limited our data range to MY 32, 34 and 35 from Ls 180-280 and 0°-70°N latitude. The latitude vs Ls position with color representing LST for MY 32, 34 and 35 in figure 1d. The ovals are added to highlight the northern winter season that is the focus of study for this paper.

Helium data from Martian years during which dust storms are only small regional storms (constrained to just the southern hemisphere or are short lived) were compared to the MY 34 global dust storm event. The He densities were found to be substantially lower during the global dust event where the bulge should have been observed (figure 4&5). Mars Global Ionosphere Thermosphere Model (M-GITM) (Bougher, et al., 2015) numerical model simulations demonstrated that under normal circumstances during northern winter (Ls ~180-240) a He bulge should form in the upper latitudes (lat ~50-70°) and night to dawn sectors (LST ~20-6h) (Elrod, et al., 2017). MAVEN NGIMS began observations during the PEDE at mid-latitudes and on the dawn-side at mid to low latitudes (~20° – 35°) moving to dusk/night (LST ~15-3h; lat 35-65°).

2. Methods

2.1 Dataset Collection

MAVEN has an inclined orbit with a periapsis of ~150 km from 2014-2020; this periapsis was then raised to ~180-200 km after Aug 2020 (mid MY 35). NGIMS is an in-situ mass spectrometer that takes measurements of the upper atmosphere during periapsis from below ~500 km (Mahaffy, et al., 2015; Stone S. W., et al., 2022). These orbits and measurements allow NGIMS to vary observation between all local times and latitudes throughout the Martian year.

Due to the limit of observations, and the fact that dust storm season typically occurs around Ls ~180-290, we needed to select data from the northern hemisphere, latitudes >45° and preferably also after 18h and before 6h local solar time (LST). MAVEN/NGIMS had this orientation during MY 32, 34 and 35. In MY 33 the spacecraft was in the southern hemisphere for Ls ~200-360 and unable to observe the He bulge (figure 1d).

While the higher altitudes have not been ideal for study of the Martian upper atmosphere, NGIMS has continued to conduct regular science. The higher altitude measurements had an impact on the heavier species (CO_2, Ar and O) measurements, but since He is a light element and has a large-scale height (nearly vertical density variation), the higher altitude measurements had little impact. Due to its large scale height, the He densities measured between 175km and 220km are very similar in the thermosphere. For this reason, we used data from 170km – 225km from MY 32, 34 and 35 for coverage and for better statistics. Since the PEDE began at Ls ~180 and extended through Ls ~240, and since the He bulge should be forming in the northern polar region as this is near northern winter, we restricted our data to this range and latitude 0-70°N.

The NGIMS density data is obtained from the level 2 closed source neutral files (version 8 revision 6) available on the PDS. The NGIMS temperature data is obtained from the scale height derived Ar density profiles from the level 3 product (version 6 revision 2) also available on the PDS. NGIMS derives the Ar scale heights using the inbound Ar densities from 165-195 km. this range was modified after the periapsis raised in Aug of 2020 to 185-220km and an additional flag was included to indicate when there were insufficient densities, or the scale heights were computed with very high error. We excluded these temperature data from our

study. This only impacted the MY 35 temperature data in figure 1c. We only included the inbound He densities as per recommendation by the NGIMS team due to instrument effects on the outbound densities.

2.2 Modeling

A three-dimensional (3D) General Circulation Model is employed to address the structure and dynamics of the upper atmosphere Mars, with the immediate objective of simulating the helium distribution as it varies with season and dust conditions. Specifically, the existing Mars Global Ionosphere-Thermosphere Model (M-GITM) is utilized to solve the Navier-Stokes equations for energy, momentum, and neutral composition on a regular spherical grid (5x5 degree horizontal resolution and 2.5 km vertical resolution over 120 levels). This Mars GITM model now combines the terrestrial GITM framework (e.g., Ridley, et al., 2006) with unique Mars fundamental physical parameters, specific ion-neutral chemistry, and essential CO_2 radiative processes in order to simulate the observed global features of the thermal, compositional, and dynamical structure of the Mars atmosphere up to ~300 km (e.g., Bougher, et al., 2015).

The M-GITM code now simulates the conditions of the Martian atmosphere near the traditional exobase all the way to the surface (Bougher, et al., 2015). Thermal and chemical drivers are carefully incorporated into M-GITM. For instance, a state-of-the-art correlated k-radiation code was adapted from the legacy NASA Ames Mars General Circulation Model (MGCM) (Haberle, et al., 2013) for incorporation into the M-GITM lower atmosphere below ~80 km. This provides solar heating (long and short wavelength), aerosol heating (seasonally

variable), and CO_2 15-micron cooling in the local thermal equilibrium (LTE) region of the Mars atmosphere. Conversely, a modern CO_2 non-local thermal equilibrium (NLTE) 15-μm cooling scheme was implemented (e.g., González-Galindo, et al., 2013) within M-GITM for the upper atmosphere (~80-250 km). External solar fluxes are taken from the MAVEN Extreme ultra-violet monitor (EUVM) via the corresponding Flare Irradiance Spectrum Model (Mars) (FISM-M). This empirical model provides 1-195-nm solar fluxes on a daily cadence throughout the MAVEN mission (Theimann, et al., 2017). The resulting M-GITM thermospheric heating, dissociation and ionization rates are simulated at each model time step (e.g., Bougher, et al., 2015).

A few other parameters, formulations, and needed boundary conditions are important to describe as well. Eddy diffusion in the model is prescribed as a globally uniform pressure-based vertical profile that yields a maximum eddy coefficient (~1000 m^2/sec) in the thermosphere and a minimum value (~500 m^2/sec) in the middle atmosphere and below (Bougher, et al., 2015). Important boundary conditions include those at the top of the model (near the exobase) and at the surface (Bougher, et al., 2015). Topside conditions allow vertical density gradients to be continuous, consistent with molecular diffusion; a non-zero flux boundary condition is thereby maintained. In addition, topside temperatures are specified to be isothermal, in accord with the exobase approximation. At the surface, densities are specified from empirical estimations, along with observed diurnal and seasonal variations for temperatures. In addition, surface thermal inertia and albedo are prescribed from 2-D maps utilized in the NASA MGCM legacy model (e.g., Haberle et al 2013).

It is clear from both observations and modeling studies that the Mars upper atmosphere is greatly impacted by waves of various spatial and temporal scales propagating upwards from the lower atmosphere (e.g., Medvedev & Yiğit, E., 2012; England, et al., 2017; Forbes, et al., 2020; Yiğit, et al., 2021; Roeten K. J., et al., 2022b; Yiğit E., 2023; Leelavathi, et al., 2020). Investigating the interaction of these waves with dust storms is essential for expanding our understanding of the vertical coupling (i.e., energy, momentum, and mass exchange between atmospheric layers) of the lower and upper atmospheres of Mars (Yiğit E., 2023; Leelavathi, et al., 2020). For this paper, we address gravity wave impacts within the M-GITM framework during the PEDE-2018 dust storm.

For this PEDE study, a simulation without gravity wave (GW) effects is conducted first. The setup for this simulation is as follows. The period for capturing the PEDE storm is targeted from June through July 2018, which includes the ramp-up, peak, and initial decay phase of the storm (see Kass, et al., 2020). Model inputs for time varying solar EUV-UV fluxes are taken from the FISM-M empirical model (Theimann, et al., 2017), which includes Mars seasonal variations. Model inputs for time varying dust optical depths and dust mixing ratio distributions are taken from MRO Mars Climate Sounder (MCS) datasets (Kass, et al., 2020). Specifically, both zonal and sol averaged values for these parameters are extracted as a function of standard MCS pressure levels (103) and new latitude elements (36). This 2-D grid is chosen to match the latitude grid of M-GITM, while assuming that zonal averaging is a reasonable first step for our simulations. Interpolation in time between even sol intervals is conducted to provide a smooth transition between sol points for the dust distribution. Aerosol heating rates are subsequently computed based upon these specified dust distributions. In addition, a simulation with GW effects is also

conducted for this PEDE study. Recently, an existing non-orographic, whole atmosphere gravity wave (GW) momentum and energy deposition scheme (e.g., Yiğit, et al., 2021; Medvedev & Yiğit, E., 2012) was incorporated in the M-GITM code in order to examine the impacts of GWs upon the thermospheric wind, density, and temperature structure (see Roeten K. J., et al., 2022b). Adding schemes to parameterize unresolved physical phenomena, such as GWs, is a common approach for relatively low-resolution global models like M-GITM. Under typical (non-dust storm) conditions, it was previously reported that with the addition of this GW scheme into M-GITM, simulated global winds can be reduced by a factor of two, and temperatures are generally cooled at all latitudes at thermosphere heights, but especially at high latitudes (Roeten K. J., et al., 2022a; Roeten K. J., et al., 2022b), compared to simulations without the scheme.

Since the addition of GW effects into M-GITM was found to produce large impacts on the modeled general circulation, a M-GITM simulation during the PEDE which utilizes the same GW scheme was also examined here to see if there are any substantial differences in the He distribution. Previously (e.g., Roeten K. J., et al., 2022b), it was found that the key adjustable GW parameters to specify for driving the GW code were the: (a) horizontal wavelength, (b) source momentum flux, and (c) launching level for these GWs near the top of the planetary boundary layer (PBL). The last two of these parameters may change over the course of the evolution of a global dust storm (i.e., yielding reduced GW forcing in the lower atmosphere), and when coupled with more favorable vertical propagation conditions (due to aerosol heating) lead to larger GW activity observed at thermospheric altitudes at the peak of the PEDE storm (e.g. Yiğit, et al. 2021). Nevertheless, as a baseline for our investigation, M-GTIM simulations in

the current analysis utilize the static GW parameters previously specified in M-GITM simulations: (e.g., horizontal wavelength = 300 km; maximum momentum flux at the source level = 0.0025 m^2/s^2; and the source level height at the top of a mean PBL = 8.0 km) (Roeten K. J., et al., 2019; Roeten & Bougher, 2022)

3. Data Analysis and Results

3.1 Analysis

In figure 1a we plot the He density at ~200km from MY 32 (grey diamonds), 34 (red stars), and 35 (dark grey triangles). Due to the high orbit to orbit variability, in order help guide the eye to pick out the peak, the black line in each data set represents the running 10-orbit average. The blue highlighted oval is the northern winter region from Ls 180-240 that is the focus of interest for this paper. This region is blown up in figure 1b and 1c. This oval corresponds to the ovals in figure 1d representing northern winter for each MY. Figure 1b is the NGIMS density data in a 10-orbit average from Ls 180-290 for MY 32 (grey diamonds) MY 34 (red stars) and MY 35 (dark triangles). The error bars are for the standard deviation of the mean, this is higher than the single error of the data in one orbit, though both have been accounted for in these error bars. Figure 1c is the NGIMS temperature in a 10-orbit average for MY 32 (grey diamonds) MY 34 (red stars) and MY 35 (dark triangles). The error bars are for the standard deviation of the orbit-to-orbit variation about the 10-orbit mean. This error accounts for the single orbit variation as well which is less than the orbit-to-orbit variation at this altitude. Figure 1d is the latitude, Ls and LST positional data for NGIMS for MY 32, 34, and 35. The key for this paper is that MY 34 was observing in the northern hemisphere from dawn

through the nightside (~6h-~20h) during Ls 180-240. MY 32 and 35 both were observing in the same hemisphere and either also had observation on the night or dawn side and thus were able to observe the He bulge during those years.

The 10-orbit average was not used for the data binning in figure 4 and 5 when comparing the NGIMS data to the model. Each orbit was binned by 5° latitude and 0.5h LST for figures 4 and 5 to compare with the M-GITM data. Model data was binned in the same manner and for figure 4 and 5 and the M-GITM data was reduced to keeping only the matching data from bins that also contained observational data.

There is a distinctly different pattern in the densities for MY 34 during the PEDE (Ls ~240-260), for which the He density is lower where there is a measured increase observed in MY 32 and 35 due to the typical He bulge (figure 1b). In addition, the MY 34 temperatures are higher on the nightside (LST 22-24h) and dawn (LST 2-6h) region compared to the other MY's at the same latitude and LST (figure 1). The higher MY 35 temperatures are from the lower latitudes and dayside. All densities are from the inbound portion of the orbit segment and are measured at ~200km altitude (Gupta et al., 2021; Elrod, et al., 2017).

Figure 2 shows the M-GITM modeling of the He neutral densities from Ls ~180 - 240 near the time of the PEDE in MY 34. Figure 2a is the M-GITM model without including gravity waves (described below), including the dust levels as observed by MRO/MCS (Kass, et al., 2020). Figure 2b is the M-GITM model that includes gravity waves (described below) Our original M-GITM modeling efforts have been shown to have a good match to the NGIMS He densities in MY 32—36 with the exception of MY 34 as shown in Gupta et al., (2021) and Elrod et al., (2017) especially for the high latitudes and winter hemisphere. However, Gupta et al., (2021)

demonstrated that near the equatorial and MY 34 densities did not agree well with the M-GITM data indicating that the M-GITM model needed revision, which we concluded was best served by the inclusion of GW's as shown in figure 2. The M-GITM model without gravity waves (figure 2a) matches reasonably well with the data observed in MY 32 and MY 35 at high latitudes during the winter season (Gupta, et al., 2021; Elrod, et al., 2017). Figure 4&5 (described below) compare the M-GITM model both with gravity waves and without. The NGIMS data in figure 1b indicate a substantial change in the He distribution in the northern hemisphere during the northern winter season.

We examined the impacts on the global circulation by conducting M-GITM simulations for MY 34 during the PEDE from its onset at Ls ~184 to its peak (Ls ~208—210) and through the early decay phase (Ls ~240). We compared this with the observed NGIMS data available through the period. We ran the M-GITM simulation with for solar forcing, globally uniform eddy diffusion parameters, and an evolving dust distribution that matches MRO/MCS dust measurements during the evolution of the PEDE but without gravity waves (figure 2a). We referred to this version of the model as the M-GITM without gravity waves and then compared the model density results to the data in figure 5, the temperature results in figure 6. The M-GITM computed He bulge is larger than expected near the dawn region above ~50°N latitude. The simulated He bulge after midnight is also too large, with a much bigger difference to the data results. In short, M-GITM meridional and zonal winds appear to be too strong in this vicinity (Miyamoto, et al., 2021; Roeten K. J., et al., 2022b).

We then revised the M-GITM model to include the addition of the new non-orographic gravity wave momentum and energy deposition scheme previously described (Roeten K. J., et

al., 2022b). This is referred to as the M-GITM with gravity waves version (figure 2b). We compare the densities to the NGIMS observations in figure 4, and the temperatures in figure 6. Standard gravity wave parameters are used that are proven to be robust, but have not included any changes with season, or disruption that may have occurred specifically with this dust event. The major impact from the inclusion of the gravity waves is to slow winds (both zonal and meridional) and cool high latitude temperatures especially. The computed model vertical and meridional winds are shown in figure 3. The computed He bulge is shown to move further northward (poleward of 50°N at the dawn terminator), providing a reduction in magnitude that reasonably matched available NGIMS measurement as shown in figures 4 (with gravity waves) and 5 (without gravity waves). However, the mismatch with the post-midnight bulge indicated the simulated bulge is still much larger than the NGIMS measurements.

Figure 3 is the computed M-GITM wind velocities. 3(a) and (b) are the meridional winds from the M-GITM model (a) without gravity waves and (b) with gravity waves. The red indicates poleward direction, and the blue is equatorial direction. The bright teal region is for the zero velocity or where the winds are nearly non-existent. This is where He is most likely to collect, specifically the northern latitudes (>30°) on the dawn (1-7h). Figure 3 (c) and (d) are the computed vertical wind distributions for the M-GITM model without gravity waves (c) and with gravity waved (d). The red is for up direction and the blue is down direction. The bright teal is the zero velocity or calm winds. The He is most likely to collect in the teal region further north (>50°) and dawn (0-6h).

We acknowledge that gravity waves could be evolving (i.e., non-constant) throughout the PEDE storm (Yiğit, et al., 2021), yet our current GW modeling is presently limited to

unchanging gravity wave parameters. We plan to make this revision in future efforts to determine how variable gravity waves are impacting the He bulge during the PEDE.

3.2 Results

Figure 4 (a, b, and c) compare the NGIMS density data with the M-GITM computed densities without gravity waves. The M-GITM output are binned by the NGIMS trajectory through the dust event (Ls ~180-240). Figure 4 plots the M-GITM density data that is binned with the NGIMS density data. Figure 4a plots the NGIMS $\log_{10}$ density (b) plots the M-GITM computed densities and (c) the $\log_{10}$ of the difference factor of the NGIMS data and the M-GITM model with gravity waves $\log_{10}(|\text{data-model}|)/\text{data}$. We chose to take the log of the difference factor because the difference between the region that matches reasonably well and that which doesn't, was large and this was the best way to be able to see the variations in the difference factor.

Figure 5 (a, b, and c) compares the NGIMS density with the M-GITM computed densities with gravity waves. The $\log_{10}$ NGIMS density is plotted in figure 5a, with the $\log_{10}$ M-GITM computed densities binned to the NGIMS observed densities in figure 5b. Figure 5c is the $\log_{10}$ difference factor for the NGIMS data and the M-GITM model without gravity waves $\log_{10}(|\text{data-model}|)/\text{data}$. We chose to take the log of the difference factor because the difference between the region that matches reasonably well and that which doesn't, was large and this was the best way to be able to see the variations in the difference factor. Both figures 4c and 5c are on the same scale. While figure 4b and 5b are not on the same scale.

The NGIMS data matches best with the M-GITM model that was revised to include gravity waves. The data and the model agrees well for latitudes below 50° latitude and dawn (LST 1-5h). The comparison between the model without the gravity waves and NGIMS data matches better for above 50° latitude and night (LST 22-24h). Because the comparison with the densities are much better with the M-GITM gravity wave, this indicates that gravity waves play a critical role. However, the fact that there is large discrepancy above 50° N latitude and on the night side (LST 22-24h). indicates that throughout the dust storm gravity waves possibly need variability in the implementation.

The densities in the computed M-GITM model which include gravity wave effects match the NGIMS density data much better on the dawn side (LST ~1-5h) and in the mid to high latitudes (~0-50°N lat). But once the spacecraft move closer to midnight and above 50°N the mismatch between the model and data become much greater. This was also where the model predicted the presence of the He bulge should be able to be observed. NGIMS did not observe a significant increase in the He data above 50°N latitude on the nightside around midnight (LST ~22h – 24h).

Figure 6 (a, b, c, d, e, and f) compares the NGIMS measured temperatures (a) with the computed M-GITM modeled temperatures without gravity waves (b) and with gravity waves (c) with during the dust event. The M-GITM model data has been binned to correspond with the NGIMS data without gravity waves in (d) and with gravity waves in (e) and the difference between them taken and plotted in each figure respectively. Note the scales are not the same for both (d) and (e). The temperatures do match better for the gravity wave case for the dawn (LST 1-5h) and lat 20-50° than for the non-gravity wave case. However, the case without gravity

waves matches better for the latitudes >50° and night (LST 22-24h). This indicates that the model upgrade employing gravity waves is a good improvement to the model, but that the gravity wave scheme likely needs be employed with a variable scheme throughout the dust storm.

4. Discussion

The reduced He bulge density during the PEDE in 2018 indicates that there is a change to the circulation in the upper atmosphere. While NGIMS wind measurements were obtained at the beginning and during the dust storm, the campaign averaged wind speeds were not significantly different in magnitude but were significantly different in direction. NGIMS winds measurements were limited to 2, 10-orbit passes one at the onset of the storm and a second near the end of the storm. This is rather limited data to confirm the M-GITM model given the significant variations that were measured in direction and speed from NGIMS (Roeten K. J., Bougher, Benna, & Elrod, 2022). While substantial winds are present throughout the dust storm in the upper atmosphere, large variations of these winds from orbit-to-orbit were also observed, possibly connected to increased gravity wave activity which was also observed in the thermosphere at the same time (Yiğit, et al., 2021).

NGIMS neutral data has been used to catalog gravity wave observations both on the dayside and night-side during non-dust seasons (England, et al., 2017). Yiğit et al., (2021) conducted an analysis of the gravity wave activity seen in the upper atmosphere during the PEDE by analyzing perturbations induced in the NGIMS CO_2 densities and found that thermospheric gravity wave activity doubles during the peak of the dust storm. In addition to gravity waves causing short time-scale variability, the momentum deposited by gravity waves

also modifies the middle-upper atmospheric circulation, as seen in several Global Circulation Model (GCM) studies (e.g., Medvedev & Yiğit, E. , 2012; Haberle, et al., 2013; Kuroda, et al., 2020). A modeling study examining the full impact of variations in the gravity waves on the atmospheric circulation or the He bulge has not yet been completed.

The He bulge forms in the cool and calmer parts of the atmosphere (figure 2 and 3). Therefore, the highest levels of He are found from ~2-5h LST at high latitudes during the winter season, and at mid to high latitudes from ~2-5h LST during the equinoxes (Gupta, et al., 2021; Elrod, et al., 2017). The fact that in MY 34 during the dust event this He bulge did not appear from LST 0-5h in the high latitudes indicates a change in the circulation of the upper atmosphere, that the atmosphere was warmer or that gravity waves and winds redistributed the He. Specifically due to the higher cooling effects of the GWs included in the M-GITM model, the computed high latitude temperatures are much cooler than observed but the non-GW temperatures were a slightly better match. This leads us to hypothesize that the gravity waves could vary throughout the dust storm and using a static gravity wave formulation (i.e., constant GW parameters) in the model is likely producing too much cooling.

Overall, our main conclusion thus far is that the gravity wave scheme we have employed in the M-GITM model is a significant improvement for driving a more realistic Mars thermospheric circulation (Roeten K. J., et al., 2022b). As a result, an improved picture is emerging describing how He is moving in the upper atmosphere and how the thermospheric circulation is changing during the PEDE. Gravity waves may be reducing the strength of the global thermospheric circulation and thereby improving the dawn region He bulge distribution and magnitude soon after the peak of the PEDE. However, a refined gravity wave scheme may

be needed that accounts for the time evolution of GW parameters and the resulting momentum/energy deposition impacting the circulation from the PEDE peak through the decay phase. The presently computed He bulge magnitude is too large (especially above 50°N latitude around midnight) and does not match the NGIMS observed values.

MAVEN continues to operate, and we hope to have additional observations of the upper atmosphere for the next PEDE from all the Mars assets available for the next major dust storm. Limitations with NGIMS observations, given that it is the only in-situ upper atmosphere instrument currently delivering He density, is one other factor to be considered in the distribution of the He bulge. While other Mars orbiters like Mars Orbiter Mission which has a similar instrument to NGIMS were also observing the PEDE (Rao, et al., 2020), it is unfortunately very limited in the light species observations (Bardwaj, et al., 2016).

5. Acknowledgements

6. Data Acknowledgement Statement

All MAVEN NGIMS data used in this work is publicly available on the Planetary Data System (PDS) (Elrod, Benna, & Navas, MAVEN Neutral Gas and Ion Mass Spectrometer [Dataset], 2014)).

In addition, solar fluxes used for M-GITM model simulations are taken from the MAVEN/EUVM FISM-M empirical model corresponding to a Level 3 Version 14, Revision 3 data product on the PDS (Eparvier, 2022)

Finally, the MGITM data is publicly available on the University of Michigan Deep Blue Data repository (e.g., Roeten & Bougher, 2022).

References

Bardwaj, A., Thampi, S., Das, T., Dhanya, M., Naik, N., Vajja, D., . . . K., A. (2016). On the evening time exosphere of Mars: Result from MENCA aboard Mars Orbiter Mission. *Geophys. Res. Lett.*, 43, 1962 - 1867. doi:10.1002/2016GL067707

Bougher, S., Bell, J., Bell, J., Nelli, S., McDunn, T., Murphy, J., . . . Ridley, A. (2015). Mars Global Ionosphere-Thermosphere Model: Solar cycle, seasona, and diurnal variations of the Mars upper atmosphere. *J. Geophys. Res. Planets*, 120, 311-342. doi:10.1002/2014JE004715

Elrod, M. K., Bougher, S. W., Roeten, k., Sharrar, R., & Murphy, J. (2020). Structural and Compositional Changes in the Upper Atmosphere Related to the PEDE-2018 Dust Event on Mars as Observed by MAVEN NGIMS. *Geophysical Research Letters*, 47, e2019GL084378. doi:https://doi.org/10.1029/2019GL084378

Elrod, M., Benna, M., & Navas, T. (2014). *MAVEN Neutral Gas and Ion Mass Spectrometer [Dataset]*. Retrieved from NASA Planetary Data System: doi: https://doi.org/10.17189/1518931

Elrod, M., Bougher, S., Bell, J., Mahaffy, P, Benna, M., Stone, S., . . . Jakosky, B. (2017). He bulge revealed: He and CO2 diurnal and seasonal variations in the upper atmosphere of Mars as detected by MAVEN NGIMS. *J. Geopyhs Res. Space Physics*, 122, 2564 - 2573. doi:10.1002/2016JA023482.

England, S., Liu, G., Yiğit, E., Mahaffy, P., Elrod, M., Benna, M., . . . Jakosky, B. (2017). MAVEN NGIMS observations of atmospheric gravity waves in the Martian thermosphere. *J. Geophys. Res. Space Physics*, 122, 2310– 2335. doi:10.1002/2016JA023475

Eparvier, F. G. (2022). *MAVEN EUV Modeled Data Bundle [Dataset]*. Retrieved from NASA Planetary Data System: doi: https://doi.org/10.17189/1517691

Farahat, A., Mayyasi, M., Withers, P., Dayeh, M., & Abuelgasim, A. (2021). Effects of the June 2018 global dust storm on the atmospheric composition of the Martian upper atmosphere as observed by MAVEN. *Journal of Geophysical Research: Planets*, 126, e2021JE006868. doi:https://doi.org/10.1029/2021JE006868

Felici, M., Withers, P., Smith, M. D., González-Galindo, F., Oudrhiri, K., & Kahan, D. (2020). MAVEN ROSE observations of the response of the Martian ionosphere to dust storms. *Journal of Geophysical Research: Space Physics*, 125, e2019JA027083.

Forbes, J., Zhang, X., Forget, F., Millour, E., & Kleinböhl, A. (2020). Solar tides in the middle and upper atmopshere of Mars. *Journal of Geophysical Researh: Space Physics*, 125(9), e2020JA028140. doi:https://doi.org/10.1029/2020ja028140

González-Galindo, F., Chaufray, J.-Y., López-Valverde, M. A., Gilli, G., Forget, F., Leblanc, F., . . . Yagi, M. (2013). Three-dimensional Martian ionosphere model: I. The photochemical ionosphere below 180 km. *J. Geophy. Res. Planets*, 118, 2105-2123. doi:10.1002/jgre.20150

Gupta, N., Rao, N., Bougher, S., & Elrod, M. (2021). Latitudinal and seasonal asymmetries of the helium bulge in the Martian upper atmosphere. *Journal of Geophysical Research: Planets*, 126, e2021JE006976. doi:https://doi.org/10.1029/2021JE006976

Haberle, R. M., Murphy, J. R., & Schaeffer, J. (2013). Orbital change experiments with a Mars general circulation model. *Icarus*, Volume 161, Issue 1, Pages 66-89, ISSN 0019-1035. doi:https://doi.org/10.1016/S0019-1035(02)00017-9

Jain, S., Bougher, S., Deighan, J., Schneider, N., González-Galindo, F., Stewart, A., & et al.,. (2020). Martian thermospheric warming associated with the Planet Encircling Dust Event of 2018. *Geophysical Reserve Letters*, 47, e2019GL085302. Retrieved from https://doi.org/10.1029/2019GL085302

Kass, D., Schofield, J., Kleinböhl, A., McCleese, D., Heavens, N., Shirley, J., & Steele, L. (2020). Mars Climate Sounder observation of Mars' 2018 global dust storm. *Geophysical Reserve Letters*, 47, e2019GL083931. Retrieved from https://doi.org/10.1029/2019GL083931

Kuroda, T., Medvedev, A., & Yiğit, E. (2020). Gravity wave activity in the atmosphere of Mars during the 2018 global dust storm: Simulations with a high-resolution model. *Journal of Geophysical Research: Planets*, 125 e2020JE006556. Retrieved from https://doi.org/10.1029/2020JE006556

Leelavathi, V. V., Leelavathi, V., Venkateswara, R. N., & Rao, S. (2020). Interannual variability of atmospheric gravity waves in the martian thermosphere: Effects of the 2018 planet-encircling dust event. *J. Geophys. Res. Planets*, 125, e2020JE006649. Retrieved from https://doi.org/10.1029/2020JE006649

Mahaffy, P., Benna, M., Elrod, M., Yelle, R. V., Bougher, S., Stone, S., & Jakosky, B. (2015). Structure and composition of the neutral upper atmosphere of Mars from the MAVEN NGIMS investigation. *Geophys Res. Letter*, 42, 8915-8957. doi:doi:10.1002/2015GL065329

Mayr, H., Harris, I., Hartle, R., & Hoegy, W. (1978). Diffusion model for the upper atmosphere of Venus. *J. Geophys. Res.*, 83(A9) 4411-4416. doi:doi:10.1029/JA083iA09p04411

Mayr, H., Harris, I., Neimann, H., Brinton, H., Spencer, N., Taylor, H., . . . Hunten, D. (1980). Dynamic properties of the thermosphere inferred from Pioneer Venus Mass Spectrometer measurements. *J Geophys Res.*, 85 (A13) 7814 - 7847. doi:doi:10.1029/JA085iA13p07841

Medvedev , A., & Yiğit, E. . (2012). Thermal effects of internal gravity waves in the Martian upper atmosphere. *Geophys. Res. Letter*, 39, L05201. doi: doi:10.1029/2012GL050852

Miyamoto, A., Nakagawa, H., Kuroda, T., Takami, K., Murata, I., Medvedev, A. S., & al., e. (2021). Intense zonal wind in the Martian mesosphere during the 2018 planet-encircling dust event observed by ground-based infrared heterodyne spectroscopy. *Geopyhs Res. Lett.*, 48, e2021GL092413. Retrieved from https://doi.org/10.1029/2021GL092413

Rao, Venkateswara, N., Gupta, N., & Kadhane, U. R. (2020). Enhanced densities in the Martian thermosphere associated with the 2018 planet-encircling dust event: Results from

MENCA/MOM and NGIMS/MAVEN. *Journal of Geophysical Research: Planets*, 125, e2020JE006430. Retrieved from https://doi.org/10.1029/2020JE006430

Ridley, A., Deng, Y., & Tóth, G. (2006). The global ionosphere-thermosphere model. *Journal of Atmospheric and Solar-Terrestrial Physics*, Vol 68, Issue 8, Pages 839-864. Retrieved from https://doi.org/10.1016/j.jastp.2006.01.008

Roeten, K. J., Bougher, S. W., Benna, M., & Elrod, M. K. (2022a). MAVEN/NGIMS wind observation in the Martian thermosphere during the 2018 planet encircling dust event. *Icarus*, vol 382. Retrieved from https://doi.org/10.1016/j.icarus.2022.115006

Roeten, K. J., Bougher, S. W., Benna, M., Mahaffy, P. R., Lee, Y., Pawlowski, D., & et al. (2019). MAVEN/NGIMS thermospheric neutral wind observations: Interpretation using M-GITM general circulation model. *Journal of Geophysical Research*, 124, 3283 - 3303. Retrieved from https://doi.org/10.1029/2019JE005957

Roeten, K. J., Bougher, S. W., Yiğit, E., Medvedev, A. S., Benna, M., & Elrod, M. K. (2022b). Impacts of gravity waves in the Martian thermosphere: The Mars Global Ionosphere-Thermosphere Model coupled with a whole atmosphere gravity wave scheme. *Journal of Geophysical Research: Planets*, 127, e2022JE007477. Retrieved from https://doi.org/10.1029/2022JE007477

Roeten, K., & Bougher, S. (2022). *M-GITM datasets used for a modeling study of the mean impacts of subgrid-scale gravity waves on thermospheric velocities and temperatures at Mars [Dataset]*. Retrieved from University of Michigan - Deep Blue Data: https://doi.org/20.7032/7hab-2340

Stone, S. W., Yelle, R. V., Benna, M., Elrod, M. K., & Mahaffy, P. R. (2022). Neutral composition and horizontal varitiations of the Martian upper atmosphere from MAVEN NGIMS. *Journal of Geophysical Research: Planets*, 127, e2021JE0070785. Retrieved from https://doi.org/10.1029/2021JE007085

Stone, S. W., Yelle, R. V., Benna, M., Lo, D. Y., Elrod, M. K., & Mahaffy, P. R. (2020). Hydrogen escape from Mars is driven by seasonal and dust storm transport of water. *Science*, vol 370 no 6518. Retrieved from https://doi.org/10.1126/science.aba5229

Theimann, E., Chamberlin, P., Eparvier, F., Woods, T., Bougher, S., Jakosky, B., & Templeman, B. (2017). The MAVEN EUVM spectral irradiance modle for solar viariability at Mars: Algoritms and results. *J. Geophys. Res.: Space Physics*, 122, 2748-2767. doi:doi:10.1002/2016JA023512

Wolkenberg, P., Giuranna, M., Smith, M., Grassi, D., & Amoroso, M. (2020). Similarities and differences of global dust storms in MY 25, 28, and 34. *Journal of Geophysical Research: Planets*, 125, e 2019JE006104. Retrieved from https:doi.org/10.1029/2019JE006104

Yiğit, E. (2023). Coupling and interactions across the Martian whole atmosphere system. *Nature Geoscience*, 16, 123-132. doi:https://doi.org/10.1038/s41561-022-01118-7

Yiğit, E., Medvedev, A., Benna, M., & Jakosky, B. (2021). Dust storm-enhanced gravity wave activity in the Matrian thermosphere observed by MAVEN and implications for atmospheric escape. *Geophysical Research Letters*, 48, e2020GL092095. Retrieved from https://doi.org/10.1029/2020GL092095
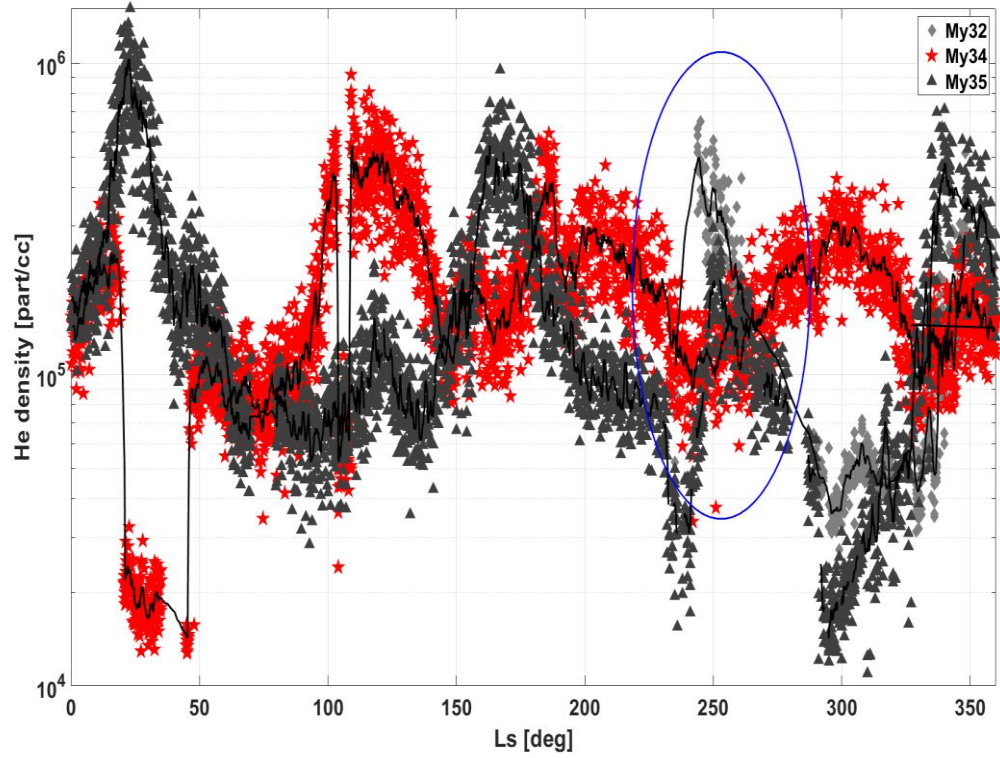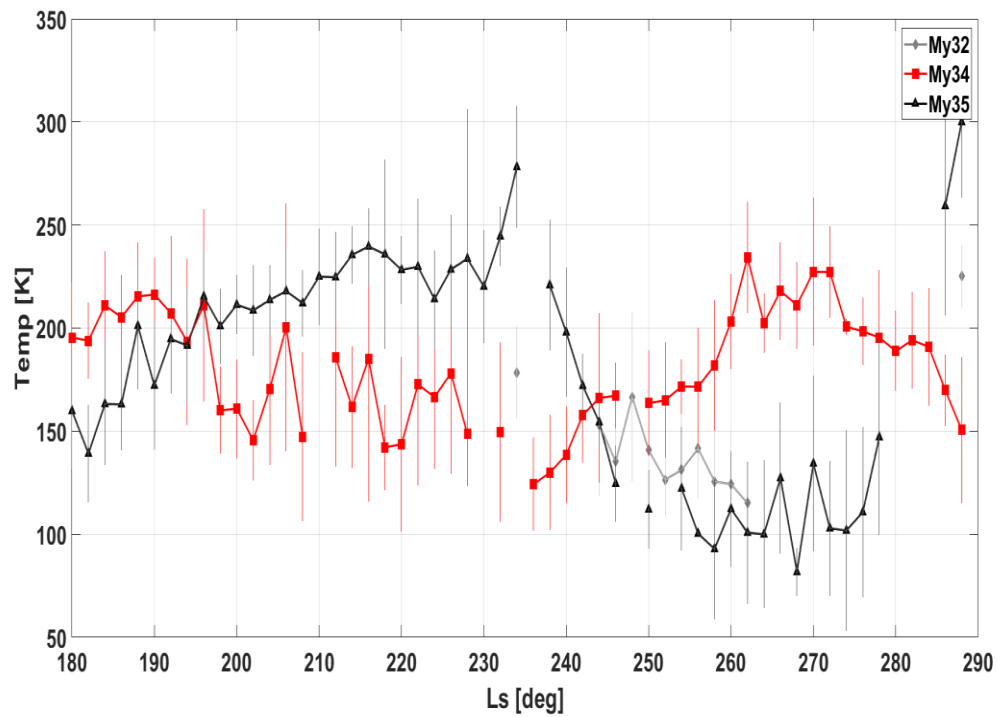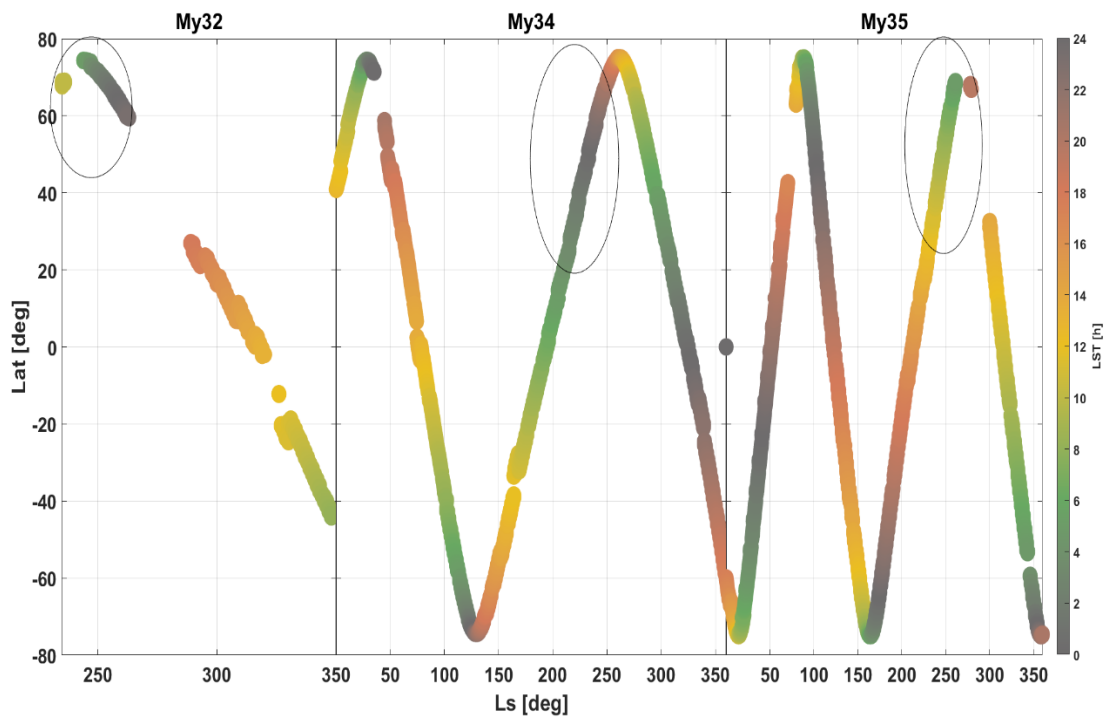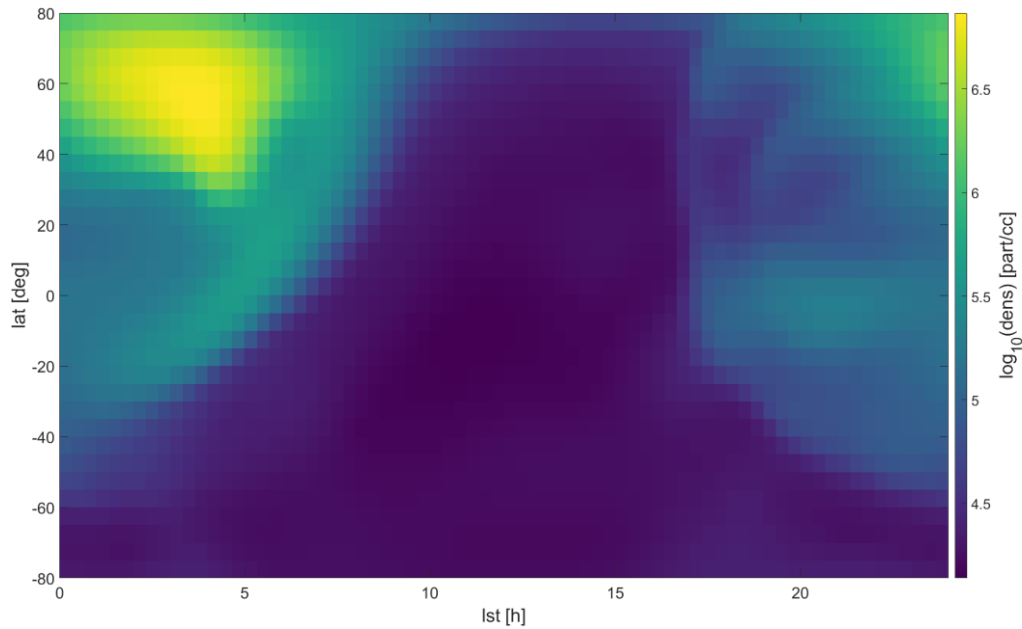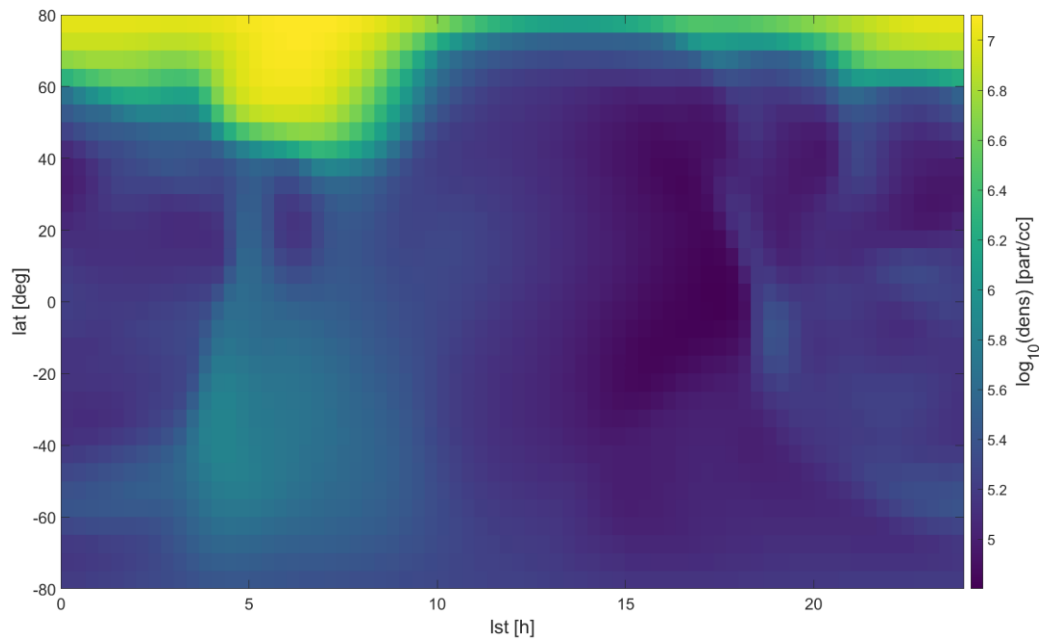
Figure 1

(a)
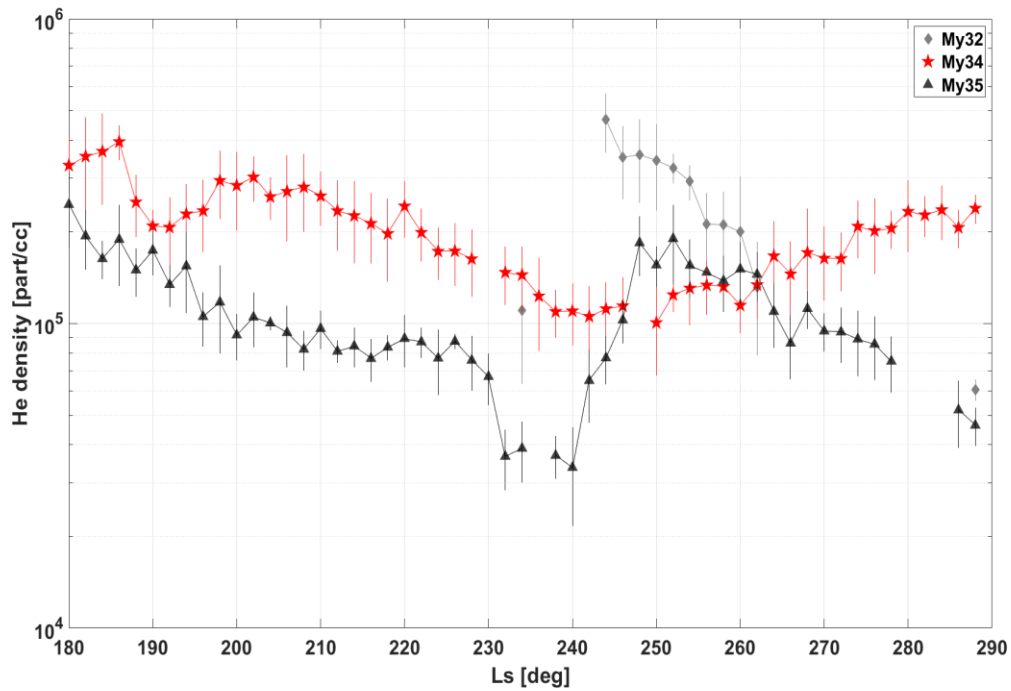
(b)

(c)

(d)

Figure 1 (a) He density [part/cc] data from MY 32 (grey diamonds), MY 34 (red stars) and MY 35 (black triangles). The solid black lines are a rolling 10-orbit average for each MY to help guide the eye and pick out the patterns in the data. The blue oval marks the northern winter solstice

and corresponds to the ovals in (d). (b)Ten-orbit average with error bars corresponding to standard deviation of the mean of the He density from Ls ~180-280 for MY 32 (grey diamonds), MY 34 (red squares) and MY 35 (black triangles). He density clearly increases as a result of observations the northern winter He bulge for MY 32 &35. In MY 34 there is no corresponding increase of He for the dawn or night northern winter latitudes. (c) Temperatures from MY 32 (light grey diamonds), MY 34 (red squares), and MY 35 (black triangles) from Ls ~180-280. The temperatures from MY 34 are warmer on the dawn and night side northern winter latitudes corresponding to where a He bulge typically forms. (d) The latitude vs orbit and local solar time (LST) of NGIMS data in MY 32, 34, and 35. The color bar indicates the LST. The ovals mark the northern winter solstice in each MY. Due the orbital precession of MAVEN, these are the only data available during northern winter through MY 36..

Figure 2

(a)

(b)

Figure 2 M-GITM computed He densities. (a) M-GITM computed density without gravity waves. The movement of the He further north and increasing between lst 20-24h above 50 deg latitude is a substantial change between the models. These are changes subject to the winds and temperatures changes. (b) M-GITM computed densities with employing gravity waves. The regular formation of the He bulge from lst 0-5h (dawn) in the northern hemisphere is similar to what was observed during MY 32 and 35.

Figure 3
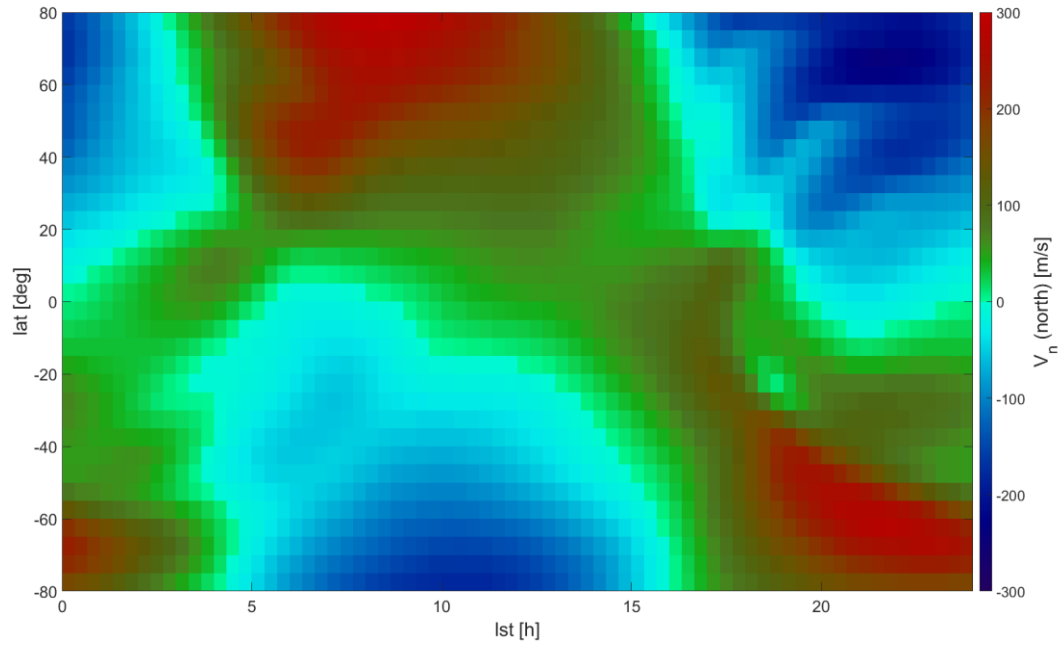
(a)
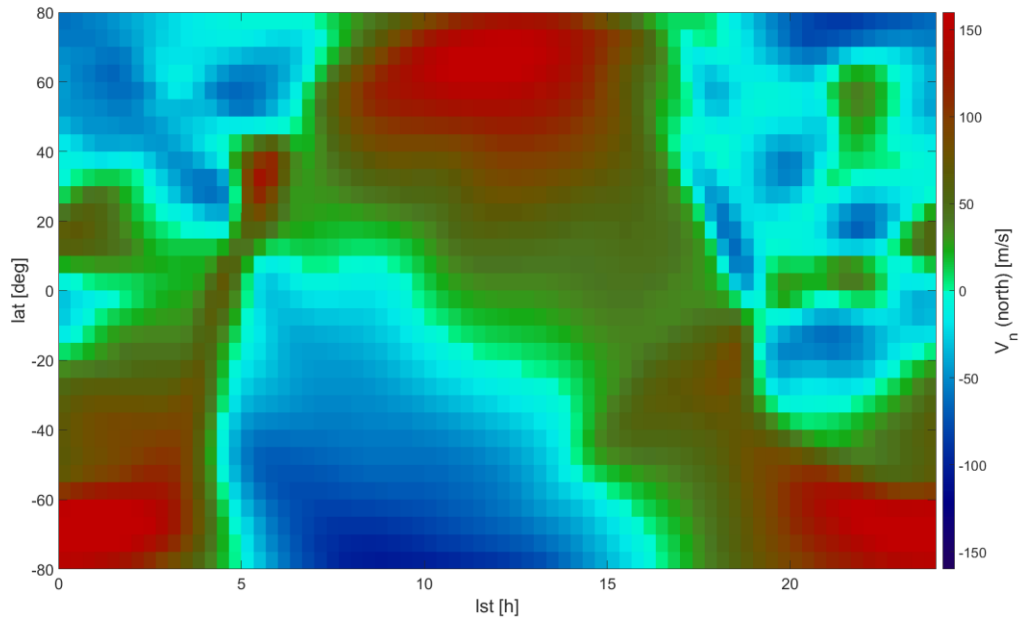
(b)
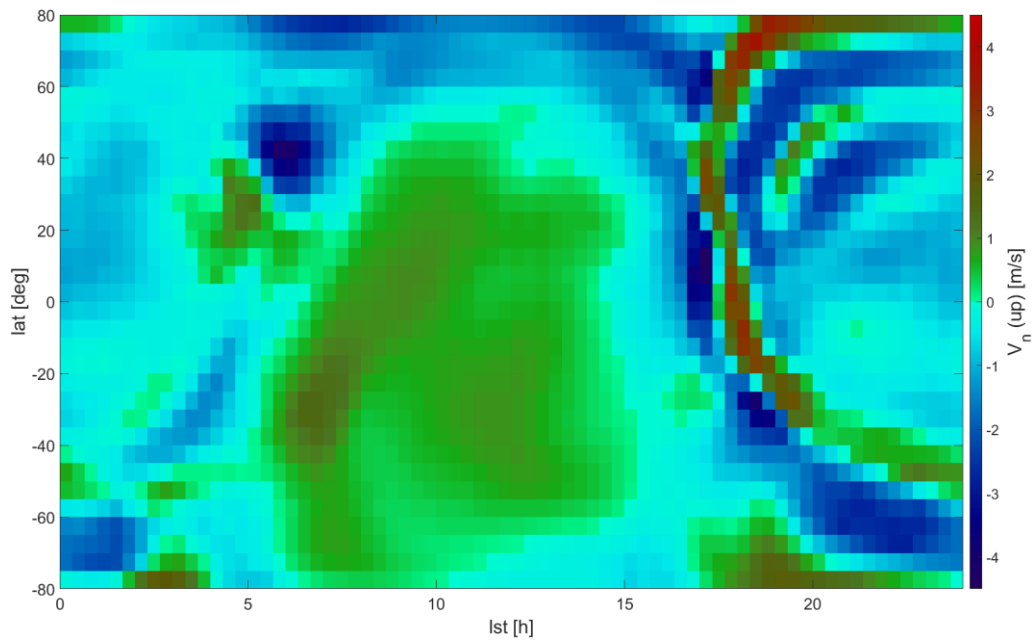
(c)
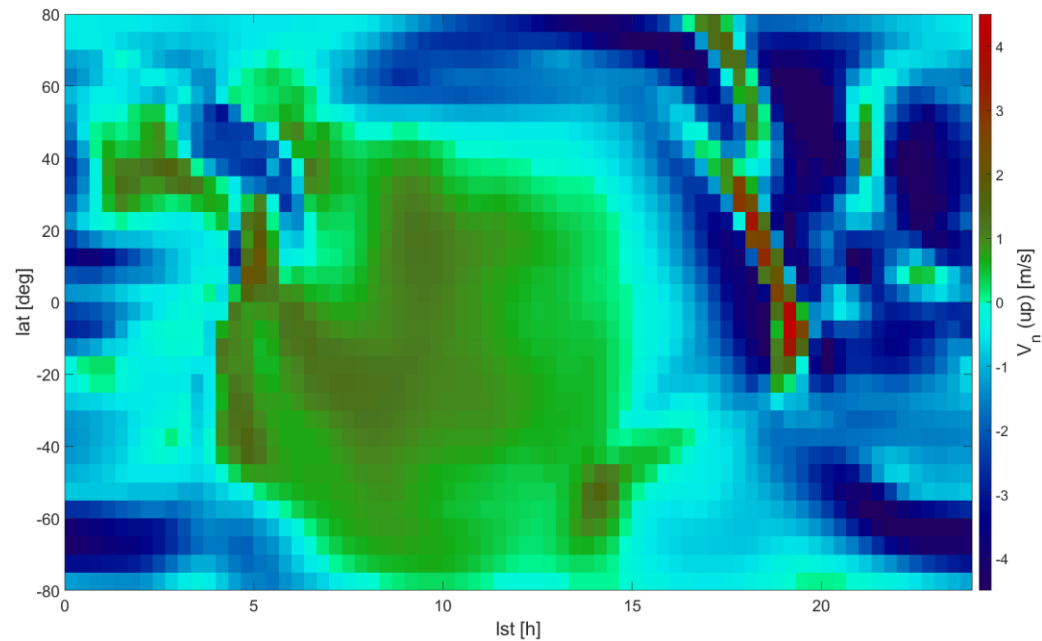
(d)

Figure 3 (a) MGTIM without gravity wave Meridional velocities and (b) MGTIM with gravity waves meridional velocities with the positive direction (red) poleward and the negative (blue) indicating equatorial. The bright teal at 0 is the zone of neutrality or calm winds. For both (a) and (b) the He is expected to collect where the low winds (bright teal) are on the dawn side. **Note the scales are different between the MGITM model with gravity waves and without**

**gravity waves as the velocities are changed significantly with gravity waves.** (c) MGITM without gravity waves vertical winds and (d) MGITM with gravity wave vertical winds. The positive direction (red) is up and the negative direction (blue) is down. The bright teal indicates 0 velocity or calm winds. Again the He is expected to collect around the teal area near the northern dawn region on the upper left side. **Note the scales are different between the MGITM model with gravity waves and without gravity waves as the velocities are changed significantly with gravity waves.**
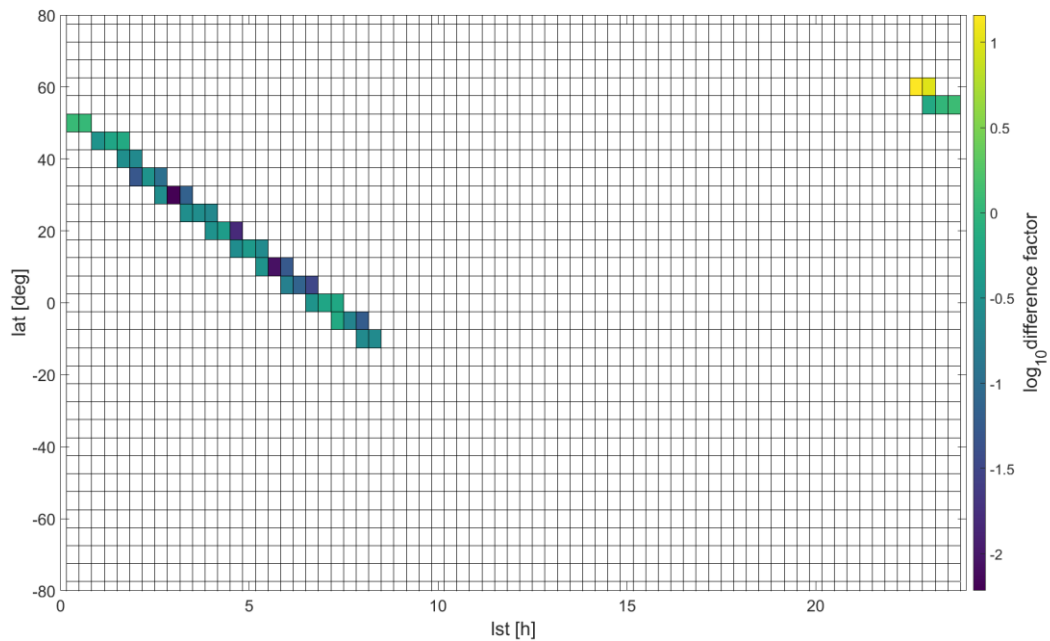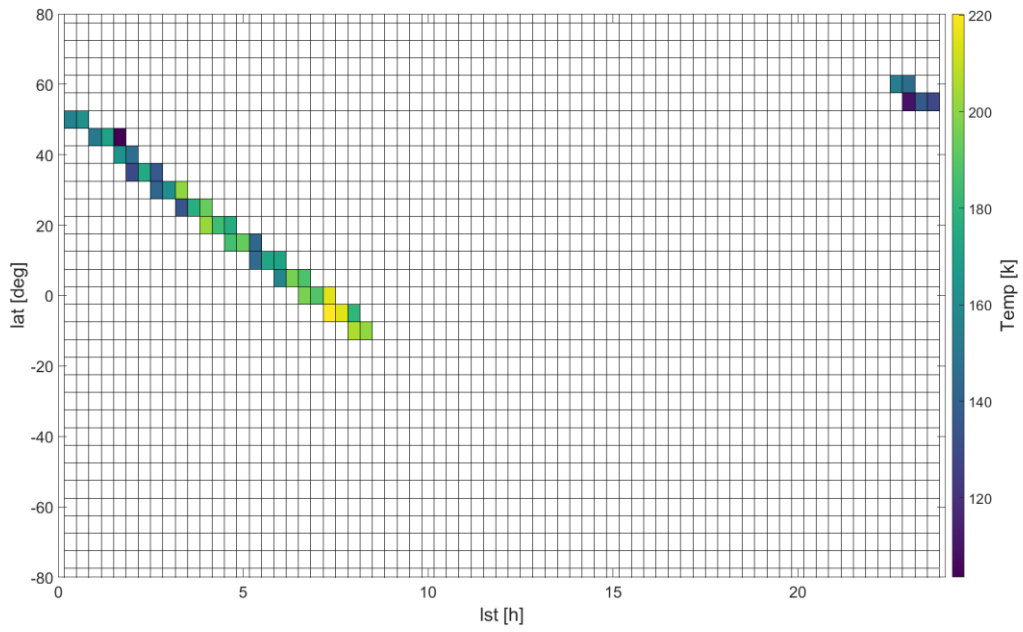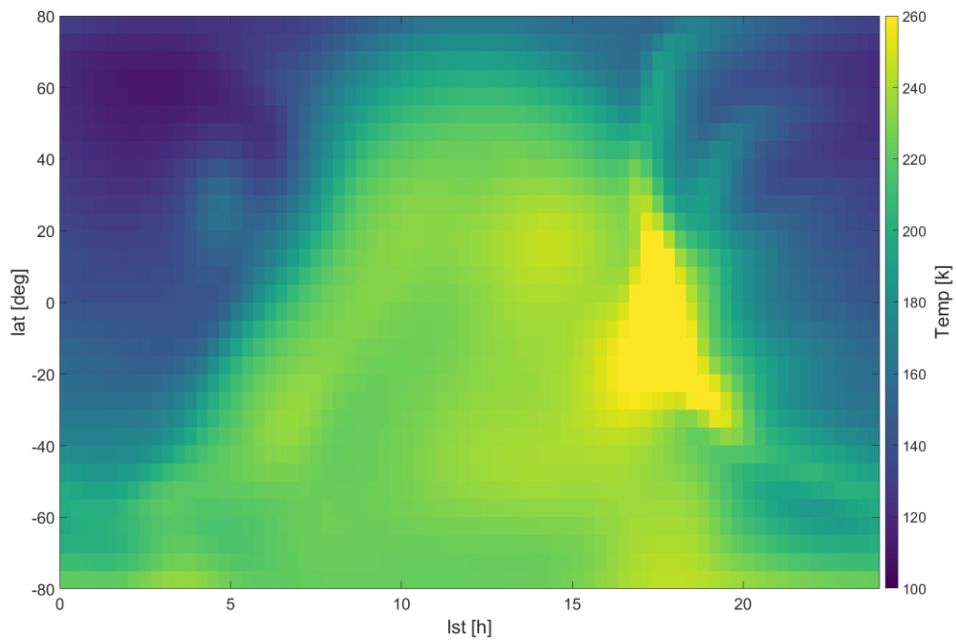
Figure 4

(a)
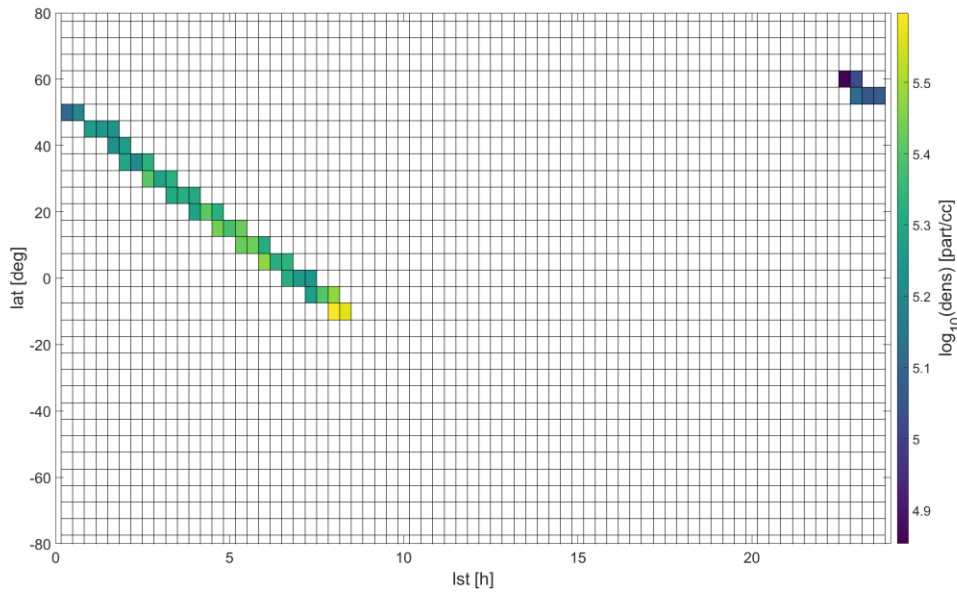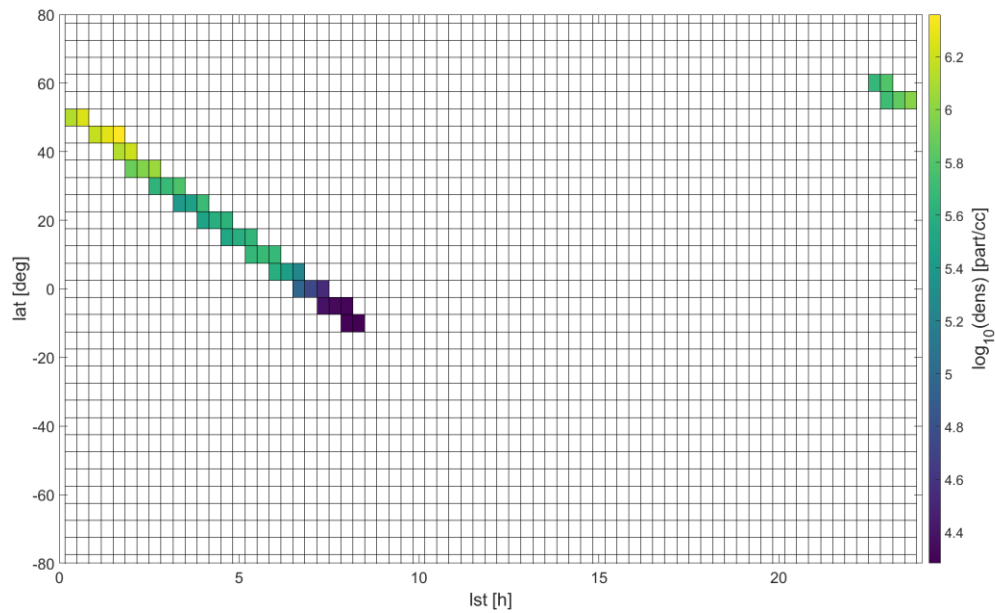
(b)
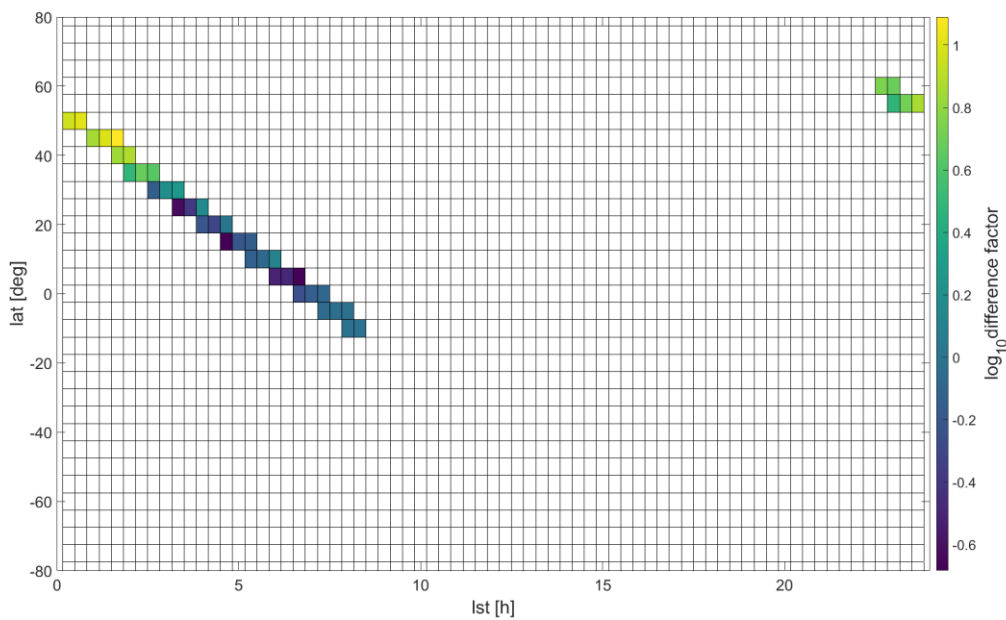
(c)

Figure 4 (a) NGIMS observed densities during the 2018 dust storm in MY 34 from Ls 180-240 at 200km inbound only. (b) MGTIM without gravity waves model data binned to match the NGIMS data during the dust storm from Ls 180-240. The He densities are plotted as a $\log_{10}$(dens) in order to bring out the variation and features. (c) The difference factor between the observed data and the model (|data – model|)/data. This is a multiplicative factor rather than a percentage as the factor was easier to plot since the numbers were high.

Figure 5
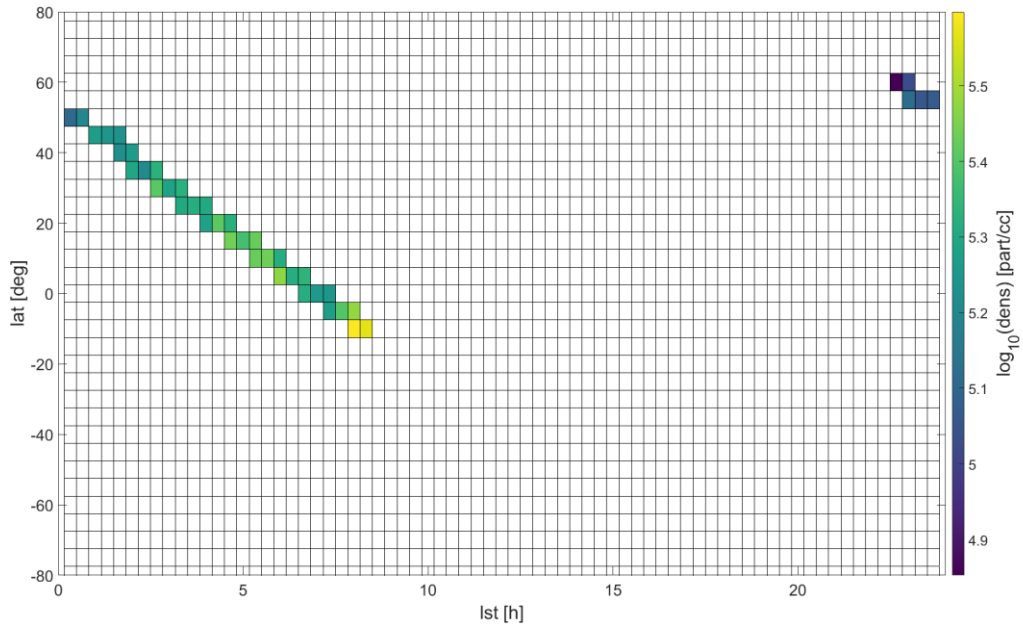
(a)
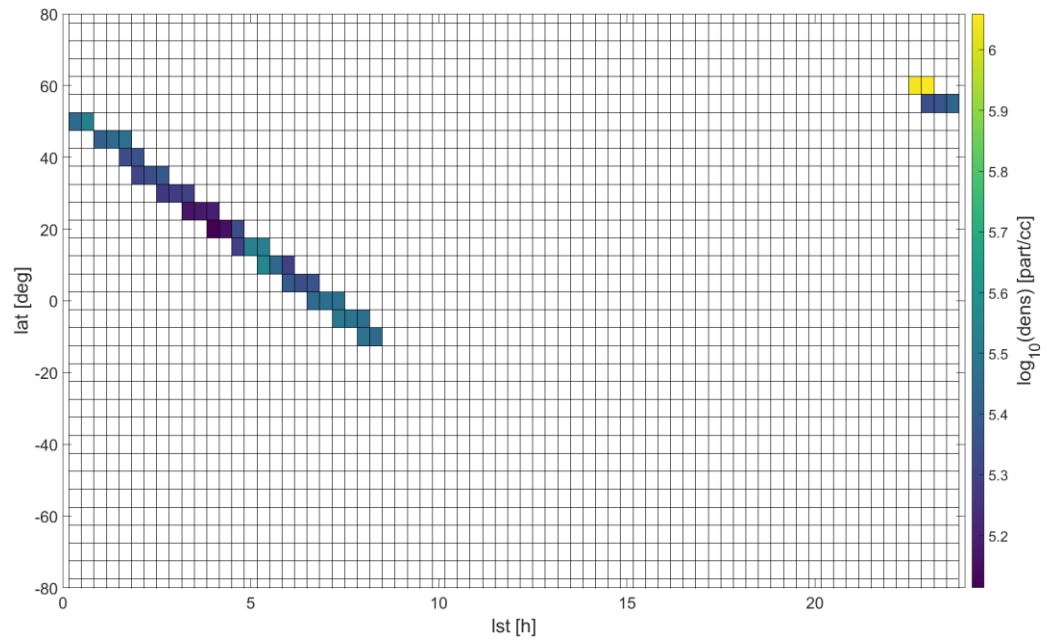
(b)

(c)

Figure 5 (a) NGIMS observed densities during the 2018 dust storm in MY 34 from Ls 180-240 at 200km inbound only. (b) MGTIM with gravity waves model data binned to match the NGIMS data during the dust storm from Ls 180-240. The He densities are plotted as a $\log_{10}(dens)$ in order to bring out the variation and features. (c) The difference factor between the observed data and the model (|data − model|)/data. This is a multiplicative factor rather than a percentage as the factor was easier to plot since the numbers were high.

Figure 6
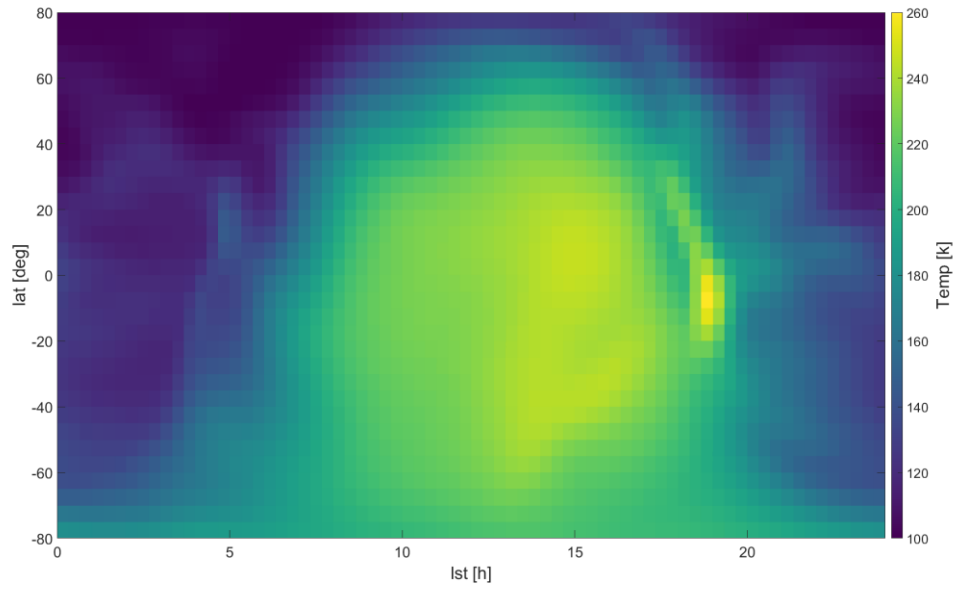
(a)
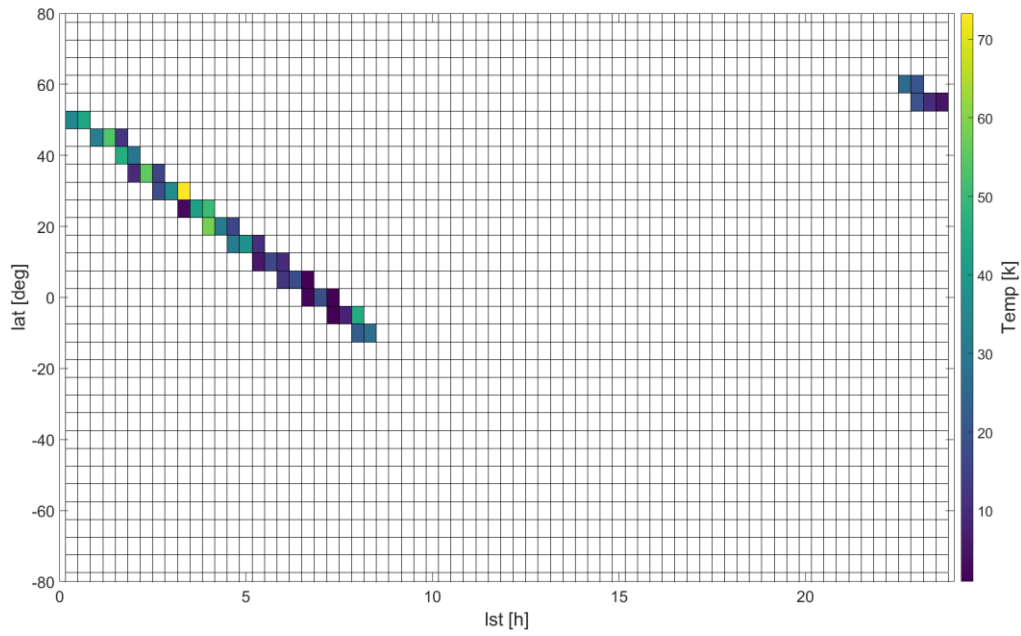

(b)
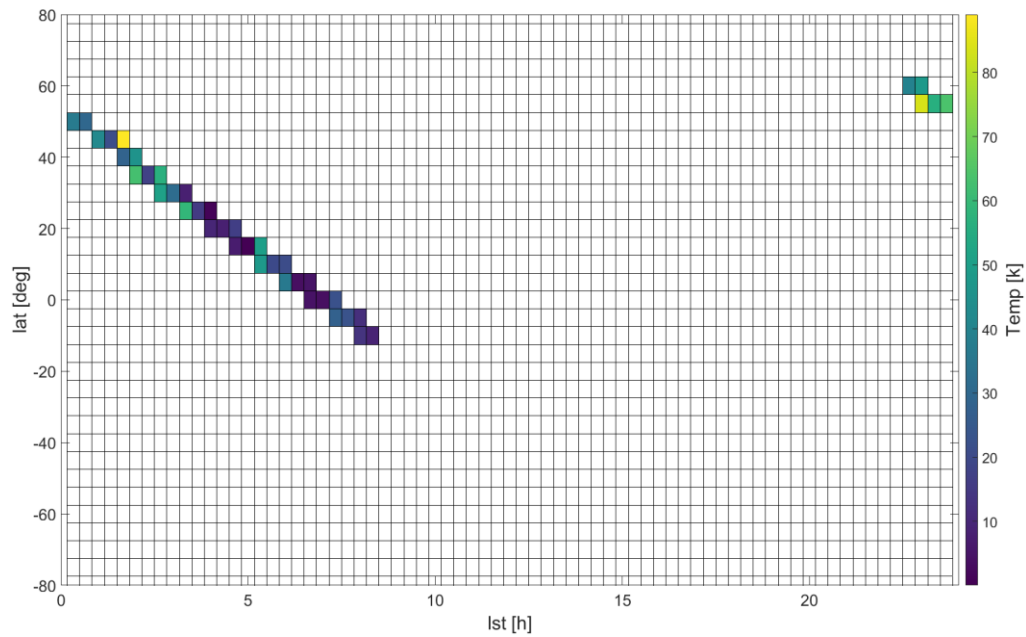
(c)

(d)

(e)

Figure 6 (a) NGIMS temperatures densities during the 2018 dust storm in MY 34 from Ls 180-240 at 200km inbound only (b) MGITM without gravity waves temperatures. (c) MGITM with gravity wave temperatures (d) Absolute temperature difference between NGIMS and MGITM without gravity waves (e) Absolute temperature difference between NGIMS and MGITM with gravity waves. Warmer temperatures and higher differences are in yellow colder and lower in blue.